Understanding and predicting the dynamics of tokamak discharges during startup and rampdown[a)]

G. L. Jackson,[1,b)] P. A. Politzer,[1] D. A. Humphreys,[1] T. A. Casper,[2,c)] A. W. Hyatt,[1] J. A. Leuer,[1] J. Lohr,[1] T. C. Luce,[1] M. A. Van Zeeland,[1] and J. H. Yu[3]
[1]*General Atomics, P.O. Box 85608, San Diego, California 92186-5608, USA*
[2]*Lawrence Livermore National Laboratory, 7000 East Avenue, Livermore, California 94550, USA*
[3]*University of California–San Diego, 9500 Gilman Drive, La Jolla, California 92093, USA*

(Received 1 December 2009; accepted 8 March 2010; published online 3 May 2010)

Understanding the dynamics of plasma startup and termination is important for present tokamaks and for predictive modeling of future burning plasma devices such as ITER. We report on experiments in the DIII-D tokamak that explore the plasma startup and rampdown phases and on the benchmarking of transport models. Key issues have been examined such as plasma initiation and burnthrough with limited inductive voltage and achieving flattop and maximum burn within the technical limits of coil systems and their actuators while maintaining the desired q profile. Successful rampdown requires scenarios consistent with technical limits, including controlled H-L transitions, while avoiding vertical instabilities, additional Ohmic transformer flux consumption, and density limit disruptions. Discharges were typically initiated with an inductive electric field typical of ITER, 0.3 V/m, most with second harmonic electron cyclotron assist. A fast framing camera was used during breakdown and burnthrough of low Z impurity charge states to study the formation physics. An improved "large aperture" ITER startup scenario was developed, and aperture reduction in rampdown was found to be essential to avoid instabilities. Current evolution using neoclassical conductivity in the CORSICA code agrees with rampup experiments, but the prediction of the temperature and internal inductance evolution using the Coppi–Tang model for electron energy transport is not yet accurate enough to allow extrapolation to future devices.
 [doi:10.1063/1.3374242]

I. INTRODUCTION

Understanding the dynamics of plasma startup and termination is important for present tokamaks and for predictive modeling of future burning plasma devices such as ITER. As device size and magnetic stored energy increase and tokamaks become increasingly complex, the implications of "off-normal" events such as failure to burnthrough low Z impurities or vertical displacement events (VDEs) have become increasingly important for the safe operation of the device. In DIII-D we have investigated the discharge evolution both to reach plasma current flattop and to ramp down the discharge to sufficiently low stored magnetic energy and plasma current where an abrupt subsequent termination does not lead to adverse effects such as erosion of plasma facing components (PFCs) or compromising the mechanical integrity of the ITER vessel. In addition, repeated abrupt terminations even at low current may have detrimental effects on these PFCs, so controlled rampdown to as low a plasma current as possible is desirable. In this paper we define burnthrough as occurring when the electron temperature becomes sufficiently high that low Z impurity charge states are no longer a large fraction of the power radiated from the plasma. This generally occurs when $T_e > 100$ eV and is characterized by a marked decrease in impurity line radiation from oxygen and carbon.

We have experimentally simulated the rampup and rampdown scenarios prescribed for the ITER tokamak and have explored variations to those prescriptions. ITER scenarios for rampup and rampdown have evolved as the machine design has matured,[1–5] and recent modeling and experiments have explored conditions for successful ITER startup and rampdown.[6–12] A typical discharge showing all phases of an ITER simulation is presented in Fig. 1. Electron cyclotron (EC) heating is used to assist in the breakdown and burnthrough phases [Fig. 1(b)], and the applied electric field is at the ITER specified value of 0.3 V/m or lower [Fig. 1(a)]. In this discharge, 1 MW of neutral beam power is applied during the rampup phase for diagnostic purposes [Fig. 1(d)]. However other ITER-like startup discharges are Ohmically ramped to current flattop under similar conditions. Neutral beam power, P_{NB}, is increased (1.6 s) after current flattop and is then feedback controlled ($\geq$1.71 s), limiting β_N to $\approx$1.7–1.8 [Fig. 1(b)]; the ITER scenario 2 value is $\beta_N = 1.8$.[13] The initial neutral beam power is well above the L-H power threshold in order to achieve a prompt L-H transition (1.67 s) since the flattop duration is limited in these experiments due to the long rampdown phase and limitations in the DIII-D power supply systems. The rampdown phase follows the ITER prescribed scenario[5] where the elongation and plasma current are simultaneously reduced and a

[a)]Paper TI3 4, Bull. Am. Phys. Soc. **54**, 255 (2009).
[b)]Invited speaker.
[c)]Present address: ITER, Route de Vinon-sur-Verdon, CS 90 046, 13067 St. Paul-lez-Durance Cedex, France.

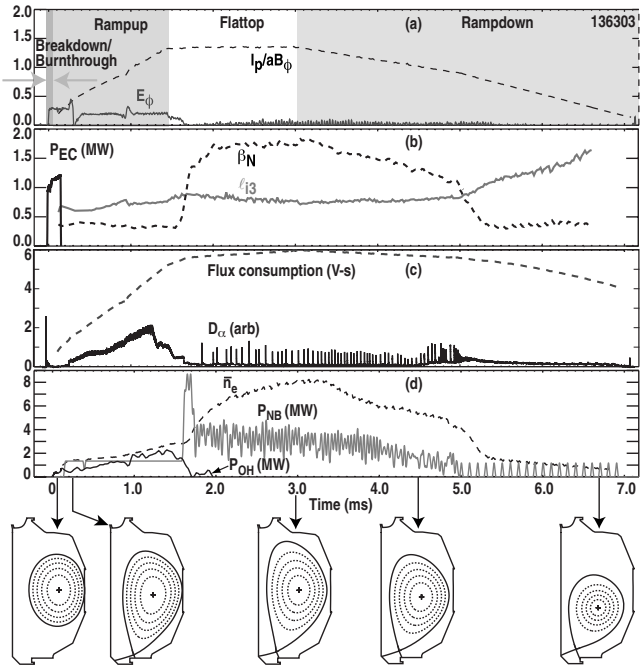

FIG. 1. DIII-D experimental simulation of a complete ITER discharge. (a) E_ϕ (V/m, solid black) and normalized current (dash); (b) normalized β (dash), $l_i(3)$ (gray) and EC power (solid black); (c) flux consumption and divertor D_α; and (d) neutral beam power (gray), OH power (solid black), and electron density ($\times 10^{19}$ cm^{-3}, dash). Discharge uses the full-bore startup scenario, diverting at 0.28 s, and the ITER prescribed rampdown scenario. Flux shapes at selected times during the discharge evolution are also shown.

transition from H-mode to L-mode occurs during the rampdown at 1.0 MA ($I_{p,ITER}=10$ MA). In this scenario, the elongation continues to be reduced during the L-mode phase, but the strike points are held approximately fixed, a key requirement in ITER for heat dissipation.

To experimentally simulate ITER startup in DIII-D, the limiter phase of the current ramp is scaled by the ratio of the low field side (LFS) radii of both devices, $R_{LFS,ITER}/R_{LFS,DIII\text{-}D}\approx 3.5$. This scaling was chosen because the initial ITER startup scenario envisaged a LFS field null and breakdown.[2] The more recent startup scenarios used in this paper include a central large-bore startup.[5,14] However, we have maintained the initial scaling of 3.5 during the limiter phase since the scaling differences are slight. During the later diverted phases, the scaling factor was set by the major radii and was 3.65. The DIII-D toroidal field, B_T, was typically 1.9–2.1 T at the major radius $R=1.7$ m (compared to 5.3 T at $R=6.2$ m in ITER). Based on gyro-Bohm scaling ($T_e \propto B_T^{2/3} a^{1/3}$), the ratio between the $L/\Re$ time in ITER and DIII-D is about 50 (L and $\Re$ are internal inductance and resistance, respectively, and a is the minor radius). Since dimensions and toroidal fields are specified, the plasma current is determined by requiring the same normalized current, $I_N=I_p/aB_T$, in both devices. For the 15 MA ITER scenario, $I_N=1.42$ and $q_{95}\approx 3$.

In the ITER baseline startup scenario, the plasma is initially limited on the LFS, and this is reproduced in DIII-D, shown in the flux plot at $t=0.1$ s in Fig. 1. In DIII-D, there are three poloidal graphite bumper limiters on the LFS, extending 2 cm from the surrounding graphite wall tiles.

During the rampup and flattop phase, the normalized internal inductance, $l_i(3)$, is within the ITER design range. In this paper we will use the definition for internal inductance used by the ITER team,

$$l_i(3) = 2V\langle B_p^2\rangle/[(\mu_0 I_p)^2 R], \quad (1)$$

where B_p is the poloidal magnetic field, $\langle B_p^2\rangle = 1/V\int B_p^2 dV$, and V is the plasma volume. The ITER design assumes an applied toroidal electric field, E_ϕ, of 0.3 V/m at $R=7.5$ m. This field is limited by induced currents in the thick vacuum vessel and poloidal field (PF) coil constraints. Although Ohmic startup has been considered for ITER, EC assist can provide an additional margin for successful breakdown and burnthrough.[1,2] For the DIII-D experiments, second harmonic X-mode (X2) EC assist was evaluated using the DIII-D 110 GHz gyrotrons. The injected power in experiments reported here was 1–1.3 MW, and the launch angle with respect to the toroidal magnetic field was varied from perpendicular launch to an oblique launch of 24 deg. (ITER has specified an oblique launch $\geq 20°$ from the equatorial EC launchers.)

For all discharges in this paper with EC assist, the EC power was applied before the inductive electric field. We define this phase as preionization and note that it has been used in a variety of tokamaks.[15–18]

In this paper we will examine the discharge phases before and after current flattop when the plasma is dynamically changing. Experiments simulating ITER flattop scenarios in DIII-D have been reported elsewhere.[13] This paper is organized as follows: Sec. II discusses the breakdown and burnthrough phases during startup, Sec. III describes the rampup phase, Sec. IV deals with rampdown, and discussion and conclusions are presented in Secs. V and VI.

II. BREAKDOWN AND BURNTHROUGH

For most experiments in DIII-D, only Ohmic heating (OH) is used for the breakdown and burnthrough phases. However, another method of startup can also be used, where EC heating (ECH) is applied and the breakdown location is determined by the EC resonance radius. Plasma breakdown and burnthrough using OH and ECH together are effective in both phases, and the higher power can make plasma initiation more reproducible and burnthrough more prompt.[18] We refer to this type of plasma startup as EC assist, and it can provide an increased margin for successful startup if used in ITER.

For OH alone, an inductive electric field of 0.8–0.9 V/m is typically applied in DIII-D discharges, providing ample power to burnthrough the charge states of low Z impurities. However, this field can be reduced to simulate ITER conditions, and an example of OH breakdown at reduced E_ϕ (0.42 V/m) is shown in Fig. 2. Even though the vacuum field null in this discharge is on the LFS, breakdown is first observed by the fast framing camera,[19] measuring D_α light, on the high field side (HFS) near the inner wall. This is consistent with Ref. 20 where the energy gain of a collisionless

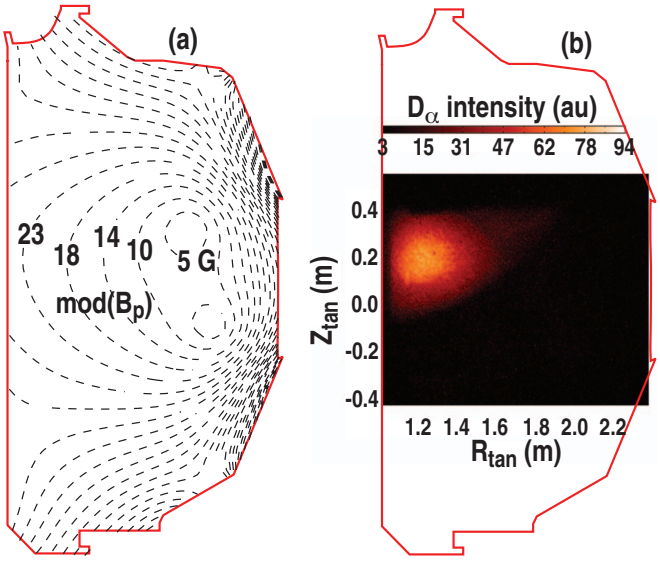

FIG. 2. (Color) Breakdown with only OH. (a) Vacuum contours of mod (B_p) in Gauss at $t=-6$ ms and (b) initial D_α intensity viewed by a fast framing camera at $t=9.3$ ms, 3 ms after breakdown, $I_p=6$ kA (No. 138138). $E_\phi=0.42$ V/m and $B_\phi=2.1$ T.

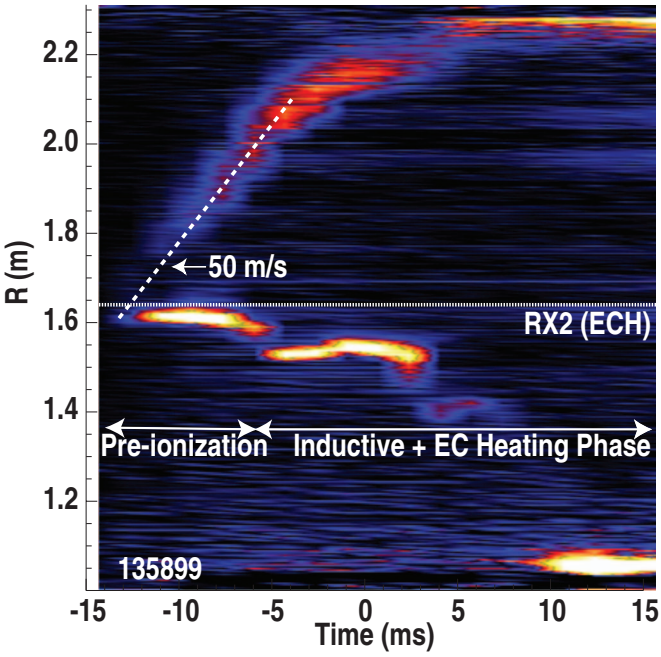

FIG. 4. (Color) Abel inversion (at $z=0$) of fast camera data in Fig. 3. EC second harmonic radius is shown as a horizontal dotted line.

electron, $U(R,z)$, following a field line from a location (R,z) inside the vacuum vessel and striking the wall is highest on the HFS near the inner wall.

Although Ohmic startup in these experiments was achieved with values as low as 0.41 V/m, it is still higher than the ITER value of 0.3 V/m. We note however that previous work with inside wall limited discharges achieved Ohmic startup with $E_\phi<0.3$ V/m.[21]

A fast framing camera viewing C^{III} line emission during startup of a discharge with EC assist is shown in Fig. 3. In the absence of an inductive electric field, plasma initiation [Fig. 3(a)] occurs near the EC X2 resonance radius, $R_{X2}=1.64$ m, and then expands toward the LFS [Figs. 3(b) and 3(c)]. The expansion is produced by a drift, $v_R=E_z\times B_\phi/|B^2|$. The electric field, E_z, is positive (upward) and is produced by charge separation due to the curvature and

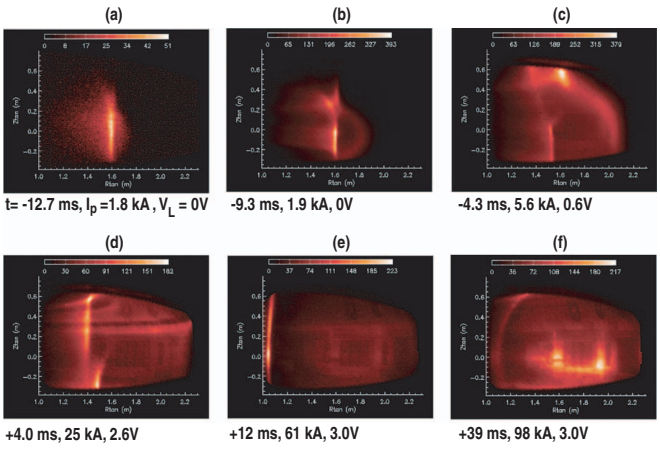

FIG. 3. (Color) Plasma formation and initial startup using a fast framing camera viewing C^{III} line emission (No. 135899). Time (millisecond), plasma current (kiloampere), and inductive loop voltage (volt) are shown at the bottom of each frame. Parameters are $B_\phi=1.9$ T and $B_z=-30$ G.

gradient drifts in the direction $B\times\nabla B$. As E_ϕ is applied [Fig. 3(d)], plasma current increases and closed flux surfaces form.[18] It is only after this time that the discharge limits on the inner wall [Fig. 3(e)] since the applied vertical field produces an inward force on the plasma. Finally, radial position feedback control is initiated beginning at $t=20$ ms, and the plasma moves to its programmed position, limiting on the LFS [Fig. 3(f)]. By this time, the plasma has completed the burnthrough phase. In these experiments, the EC power continued until $t>0.2$ s. This was done to ensure that all discharges, especially those at low ECH power (not shown), had sufficient margin for burnthrough. We would expect a successful startup (i.e., current ramp to flattop) if the EC power had been removed immediately after burnthrough for the discharge shown in Fig. 3.

The plasma expansion evolution in Fig. 3 is also shown in Fig. 4, where midplane C^{III} emission ($z=0$) is calculated from an Abel inversion. During the preionization phase ($E_\phi=0$), this expansion is nearly linear (dashed line in Fig. 4), and a radially outward velocity and electric field can be calculated, 50 m/s and 95 V/m, respectively, for discharge No. 135899 in Fig. 4. Although a detailed scan has not been carried out, we note that this velocity increases with EC power, increasing to 90 m/s when the EC power is doubled. Another interesting feature of the plasma formation is the radial expansion inward beginning at approximately -7 ms as inductive voltage is first applied. This expansion occurs in discrete steps, and the reason for this is currently under investigation.

Another feature of the EC breakdown is that a small noninductive toroidal current ≤ 6 kA is observed in discharges with EC assist as the plasma expands outward during the preionization phase. This current was measured by a "virtual" Rogowski loop consisting of a series of poloidal

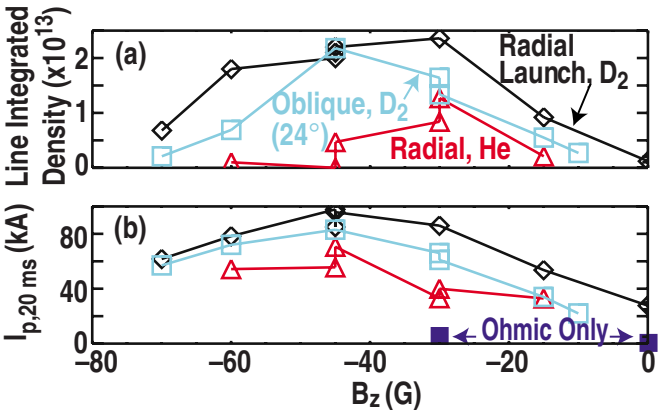

FIG. 5. (Color online) (a) Peak line integrated density during the preionization phase and (b) initial current at $t=20$ ms as a function of vertical field at breakdown. Plotted are radial EC launch with deuterium fill gas (diamond), oblique launch, 24 deg, with deuterium (square), and radial launch with helium (triangle). Two Ohmic discharges (solid squares) that did not burnthrough are also shown. Discharge conditions are $B_\phi=1.9-2.1$ T and $E_\phi=0.3$ V/m.

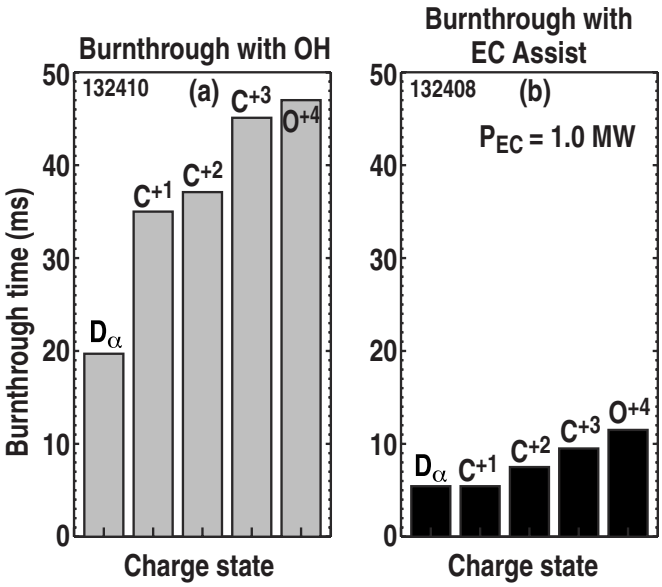

FIG. 6. Burnthrough times of selected low Z impurities for OH startup and startup with EC assist. Times are referenced to start time of heating power, either OH (a) or EC (b).

magnetic probes distributed around the inside of the vacuum vessel at a fixed toroidal location. This effect has been also been reported in other tokamaks.[17,22]

Although startup with EC assist may offer several advantages for ITER, optimized conditions can be different from those for OH alone. One important feature is that the most robust startup with EC assist requires additional vertical field when compared to OH alone. This is shown in Fig. 5 where peak preionization line integrated density and initial plasma current (measured at 20 ms) are plotted as a function of the applied vertical field, B_z (a negative value produces an inward force on the plasma). Except for the Ohmic cases in Fig. 5, these discharges had burned through the low Z impurities by 20 ms. The observation that larger $|B_z|$ is more effective is somewhat counterintuitive since it reduces the connection length of field lines to the wall (a short connection length makes ionizing collisions and hence the avalanche less probable[21]). Note that at the ITER specified value (0.3 V/m) in this scan, Ohmic burnthrough was not achieved.

In Fig. 5, both radial and oblique EC launch are compared using deuterium fueling. While radial launch had a somewhat broader range, breakdown and burnthrough occurred for both over a wide range of B_z. We note that ITER has been designed for oblique launch with a minimum angle of $\approx 20°$.

DIII-D has also examined startup in helium discharges, and a comparison of EC assist between helium and deuterium is shown in Fig. 5. The initial plasma current is lower, and preionization is observed over a narrower range of B_z, implying that startup conditions may need to be more carefully optimized in future tokamaks operating in helium.

The higher heating power available with EC assist allows the plasma to heat faster and to burn through the low Z charge states, consisting mainly of oxygen and carbon. The burnthrough time of selected charge states is plotted in Fig. 6 for both OH and EC assisted discharges. With EC assist, burnthrough time is dramatically reduced, and the more precise turn-on time of the EC gyrotrons allows more reproducible startup conditions.

III. RAMPUP OF ITER-LIKE DISCHARGES

DIII-D has experimentally simulated the rampup phase using the ITER baseline rampup scenario.[4,14] In this scenario, the plasma is initially limited on the LFS, then diverted when $I_{p,ITER}=7.5$ MA. During the rampup phase, the plasma shape is evolved to maintain q_{95} at a constant value. Since this startup scenario begins with a small volume, we refer to this as the "small-bore" scenario. During DIII-D experiments with the small-bore scenario, internal inductance was often outside the ITER specified range, and VDEs sometimes occurred, leading to disruptions.[14] In addition, ITER modeling showed that the heat flux to the LFS poloidal limiters was near engineering limits,[23] and hence a different scenario was developed with a larger plasma volume and an earlier time to divert. This scenario, referred to as the large-bore scenario, reduced potential heat flux issues and reduced internal inductance, allowing operation within the ITER specified range. To more precisely control internal inductance and operate further from the VDE threshold, feedback control of $l_i(3)$ was successfully implemented and has been reported elsewhere.[10]

Methods to reduce flux consumption are important for ITER in order to have sufficient flux for the specified burn time. Flux during the rampup phase can be reduced by the addition of modest amounts of auxiliary heating. A comparison of flux consumption with OH, neutral beam heating, and ECH is shown in Fig. 7. All three discharges had L-mode confinement, and the auxiliary heating exhibited an approximately 20% reduction in total flux required to reach current flattop. Although the temporal trajectories of $l_i(3)$ were different, all three discharges had approximately the same value

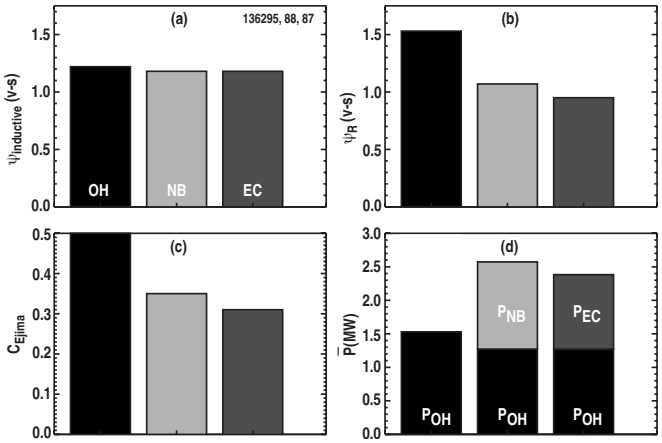

FIG. 7. (a) Comparison of flux consumption from the start of inductive voltage to current flattop for three discharges: OH only, EC, and NB during the entire current ramp. Plotted are (a) inductive flux, (b) resistive flux, (c) Ejima coefficient (defined in text), and (d) average power during the current ramp.

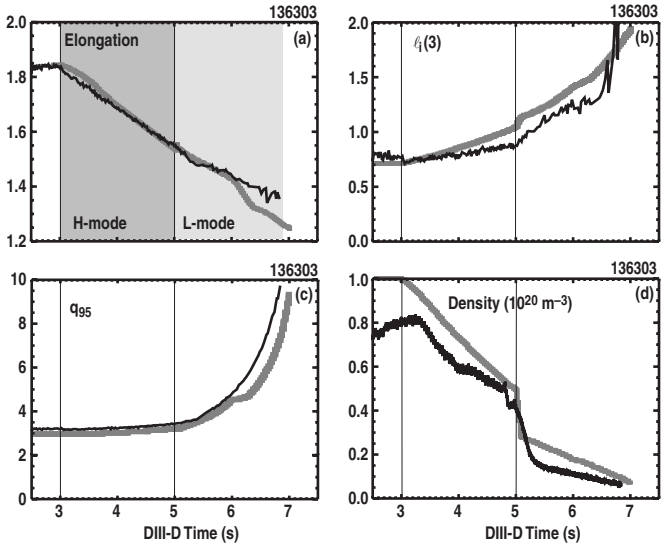

FIG. 8. Comparison of DIII-D experimental simulation of ITER (black) to ITER modeling (gray) using the DINA code. (a) Elongation, (b) q_{95}, (c) $l_i(3)$, and (d) density. [Adapted from Fig. 3 of the Institute of Publishing "Experimental Simulation of ITER Rampdown in DIII-D" (Ref. 12).]

of internal inductance at current flattop. We note that C_{Ejima} in Fig. 7(c) was also reduced with auxiliary heating. The Ejima coefficient, C_{Ejima}, is a measure of the resistive flux required, normalized to plasma current, and is given by

$$C_{\mathrm{Ejima}} = \Delta\Phi_R/\mu_0 R I_p, \tag{2}$$

where $\Delta\Phi_R$ is the resistive flux obtained by subtracting the plasma poloidal flux (calculated from the MHD equilibrium code, EFIT) from the total flux at the plasma boundary.

In order to predict the rampup performance in ITER, predictive codes need to be benchmarked with experimental data. For the DIII-D experiments described here, both the small-bore and large-bore discharges have been modeled by the CORSICA code.[24,25] CORSICA is a two-dimensional equilibrium and one-dimensional transport predictive integrated modeling code that can operate in several modes using either free-boundary or fixed-boundary solvers to simulate the discharge equilibrium evolution. For this work a Coppi–Tang transport model[26] is used with the same transport coefficients as used for ITER modeling.[11] As reported in Ref. 11, the CORSICA code accurately models the plasma current and electron temperature evolution for similar large-bore startup discharges as those presented in this paper, but there are significant differences in the current profile and internal inductance between experiment and modeling. While some of this discrepancy can be accounted for by increasing the edge temperature profile, there is still a difference, suggesting that the ITER coefficients used in the Coppi–Tang model may not be sufficiently accurate.

IV. EXPERIMENTALLY SIMULATING ITER RAMPDOWN

With the large stored energy in burning plasma devices such as ITER, safe and controlled termination of these discharges is an important aspect of their operation. In ITER, there is approximately 350 MJ of thermal energy in the $Q=10$ scenario and even more magnetic stored energy that must be controlled during the rampdown phase.[12] ITER has prescribed a rampdown scenario,[5] and this has been experimentally simulated in DIII-D. A comparison of a DIII-D ITER-like rampdown discharge and the DINA reference scenario[5] is shown in Fig. 8. With the scaling described in Sec. I, DIII-D has closely matched normalized parameters q_{95}, κ, l_{i3}, and I_n. With this scenario, rampdown to below the ITER specified value, $I_{p,\mathrm{ITER}}=1.4$ MA ($I_{p,\mathrm{DIII\text{-}D}}=0.14$ MA), was achieved. Although additional flux was not required from the entire PF set during this rampdown, additional current in the central solenoid (CS) and inner PF coils in DIII-D was required, and this might exceed the current limits of the CS coils in ITER (in DIII-D the inner CS shaping coils and the CS are decoupled, while in ITER the CS provides similar functionality). Hence alternate scenarios were investigated, with a faster current rampdown. As reported in Ref. 12, a faster rampdown produced conditions where no additional CS current was required. At the fastest L-mode rampdown rate, however, there was a disruption, and hence there is a window in current ramp rate for successful rampdown in DIII-D without requiring additional CS current.[12]

Normalized internal inductance during the current rampdown phase of a DIII-D discharge is shown in Fig. 1(b). A stability plot is presented in Fig. 9, where the controllability parameter, ΔZ_{max},[27] remains above the DIII-D control system limit (i.e., the system is stable) until I_p is well below the ITER specified value of 1.4 MA (scaled to $I_{p,\mathrm{DIII\text{-}D}}=0.14$ MA). This was achieved without using the inner PF coils in the vertical control algorithm. Normally these coils are included to provide a larger margin for vertical stability, but not using them better approximates the ITER conditions. In Fig. 9(d), the DIII-D control system stability limit is determined by system noise and control system characteristics. Despite the reduction in elongation, near the end of the rampdown, the increasing internal inductance and reduced plasma-PF coil coupling resulted in a rapidly increasing growth rate, γ_z [Fig. 9(c)]. The controllability parameter, ΔZ_{max}, decreased to below the control limit for these ITER-

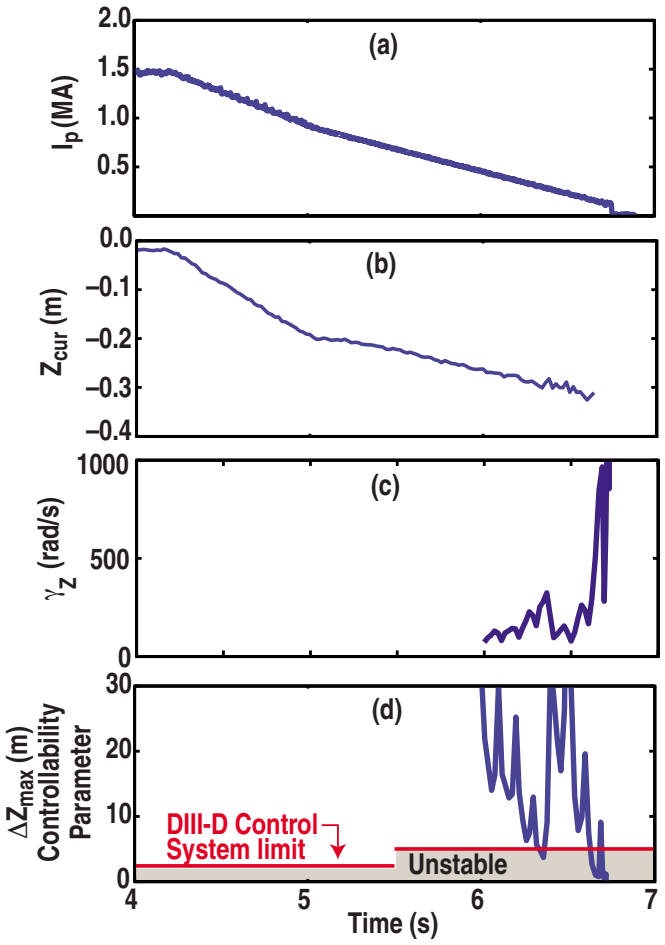

FIG. 9. (Color online) Stability analysis during rampdown (No. 136327) of an ITER-like discharge. (a) Plasma current, (b) vertical location of current centroid, z_{cur}, (c) growth rate of the $n=0$ mode, and (d) controllability parameter, ΔZ_{max}.

like operating conditions, and the system became vertically unstable. We note that during the rampdown it was necessary to change the control system algorithm in order to maintain vertical stability at low elongation with the current centroid, z_{cur}, well below the midplane. Although vertical stability was demonstrated for these DIII-D discharges, we note that simulations of the ITER control system, power supplies, and plasma models[27–30] are necessary to extrapolate these results to ITER.

V. DISCUSSION

Breakdown and burnthrough with EC assist represent an alternative method to the OH startup used in most present day tokamaks. The precise turn-on of the ECH allows a reproducible breakdown, and the additional power provided by ECH provides more rapid burnthrough when compared to OH alone, which is especially important with the lower inductive electric fields in ITER. With EC assist, reliable startup with toroidal electric fields at or below the ITER specification of 0.3 V/m has been obtained both in the work reported here and in other tokamaks.[7]

EC breakdown occurs near the EC resonance radius, and initially the plasma expands outward, toward the LFS, as contrasted with the normal OH startup near the HFS wall. In addition, there is a faster rise in plasma current with EC assist, allowing less flux consumption during the plasma formation phase. We note that a noninductive toroidal plasma current has also been observed in the preionization phase. While the value is rather modest, ≤ 6 kA, by properly phasing its evolution with respect to the start of the inductive voltage, it might provide a target current that would allow more rapid plasma formation and could further reduce flux consumption and improve reproducibility in ITER. The physical mechanisms for this noninductive startup current have not been clearly identified nor has the maximum current been optimized. Two mechanisms are currently under consideration: trapped particle effects and Pfirsch–Schlüter currents on open field lines.[22]

In DIII-D, EC assisted startup is reliably obtained with about 1 MW of X2 ECH. As shown in Fig. 6, burnthrough is also more prompt with the additional power provided by ECH. Previous scans of the resonance location showed that breakdown always occurred near the X2 resonance radius,[18] although the heating efficiency has not been evaluated as a function of radius. In DIII-D, the deposition location inferred from fast camera data and EFIT equilibria is well within the last closed flux surface (LCFS), and ECH is effective during startup. The type of ECH is different in ITER (fundamental O-mode), but the ITER design also assumes that the deposition location is within the LCFS.

An important feature of EC assisted startup is that it is most effective with an applied vertical field both in the breakdown phase and during the current ramp. With this applied vertical field, the plasma is limited on the inside wall as soon as closed flux surfaces form. In these experiments, radial field control is not enabled until $t=20$ ms when the plasma is limited on the LFS limiters to simulate the ITER rampup scenario. Optimizing the vertical field will also be an important consideration for EC assisted startup in ITER. Presently, the physical mechanism for improved breakdown with vertical field is not well understood. One hypothesis under investigation is that the applied vertical field allows better alignment between the EC resonance radius and a field line from the EC first-pass deposition location to the wall, which might enhance multipass ECH.

The ITER EC startup system has been designed for oblique launch, and this was compared to radial EC launch in Fig. 5. If the vertical field is optimized, then startup with EC assist is effective. We note that previous results, reported in Ref. 18, were for $B_z \approx 0$, which is qualitatively consistent with Fig. 5 where very little density is observed during preionization even with radial launch. Initial results with startup in helium show that preionization density is low for all values of vertical field and the rate of current rise is slower than in deuterium. This will be further investigated in future experiments.

Successful rampdown without additional flux consumption or increased currents in the center solenoid or CS coils has been demonstrated in a modified ITER rampdown scenario. The slow rampdown rate in the ITER prescribed scenario produced additional currents in the inner PF coils that could exceed coil current limits in ITER. Successful ramp-

down to plasma currents below the ITER specified limits with no vertical instabilities was achieved by changing the vertical stability algorithm in the DIII-D plasma control system. This was necessary because as elongation decreased while holding strike points fixed, the entire plasma is shifted downward. Multiple algorithms may also be necessary for ITER.

VI. CONCLUSIONS

All phases of an ITER discharge have been experimentally simulated in DIII-D. Two types of low inductive voltage startup have been investigated: the normal OH startup and EC assisted startup. In the former case, OH startup at the ITER specified electric field of 0.3 V/m has not yet been achieved in the ITER startup scenario. However EC assisted startup with E_ϕ as low as 0.21 V/m has been demonstrated. With EC assist, burnthrough of low Z impurities is fast, and breakdown is more reproducible. During the rampup phase, modest amounts of auxiliary heating, $\approx 1.1-1.3$ MW, has reduced total flux consumption by 20%, providing more margin for achieving the specified ITER burn time. Rampdown has been demonstrated below the ITER specified requirement of 1.4 MA ($I_{\mathrm{p,DIII\text{-}D}}=0.14$ MA). Finally, an improved ITER rampdown scenario has been demonstrated without additional flux consumption or increased current in the CS or PF coils.

ACKNOWLEDGMENTS

This work was supported by the U.S. Department of Energy under Grant Nos. DE-FC02-04ER54698, DE-AC52-07NA27344, and DE-FG02-07ER54917.

[1] R. Aymar, P. Barabaschi, and Y. Shimomura, Plasma Phys. Controlled Fusion **44**, 519 (2002).
[2] Y. Gribov, D. A. Humphreys, K. Kajiwara, E. A. Lazarus, J. B. Lister, T. Ozeki, A. Portone, M. Shimada, A. C. C. Sips, and J. C. Wesley, Nucl. Fusion **47**, S385 (2007).
[3] R. J. Hawryluk, D. J. Campbell, G. Janeschitz, P. R. Thomas, R. Albanese, R. Ambrosino, C. Bachmann, L. Baylor, M. Becoulet, I. Benfatto, J. Bialek, A. Boozer, A. Brooks, R. Budny, T. Casper, M. Cavinato, J.-J. Cordier, V. Chuyanov, E. Doyle, T. Evans, G. Federici, M. Fenstermacher, H. Fujieda, K. G'al, A. Garofalo, L. Garzotti, D. Gates, Y. Gribov, P. Heitzenroeder, T. C. Hender, N. Holtkamp, D. Humphreys, I. Hutchinson, K. Ioki, J. Johner, G. Johnson, Y. Kamada, A. Kavin, C. Kessel, R. Khayrutdinov, G. Kramer, A. Kukushkin, K. Lackner, I. Landman, P. Lang, Y. Liang, J. Linke, B. Lipschultz, A. Loarte, G. D. Loesser, C. Lowry, T. Luce, V. Lukash, S. Maruyama, M. Mattei, J. Menard, M. Merola, A. Mineev, N. Mitchell, E. Nardon, R. Nazikian, B. Nelson, C. Neumeyer, J.-K. Park, R. Pearce, R. A. Pitts, A. Polevoi, A. Portone, M. Okabayashi, P. H. Rebut, V. Riccardo, J. Roth, S. Sabbagh, G. Saibene, G. Sannazzaro, M. Schaffer, M. Shimada, A. Sen, A. Sips, C. H. Skinner, P. Snyder, R. Stambaugh, E. Strait, M. Sugihara, E. Tsitrone, J. Urano, M. Valovic, M. Wade, J. Wesley, R. White, D. G. Whyte, S. Wu, M. Wykes, and L. Zakharov, Nucl. Fusion **49**, 065012 (2009).
[4] V. Lukash, Y. Gribov, A. Kavin, R. Khayrutdinov, and M. Cavinato, Plasma Devices Oper. **13**, 143 (2005).
[5] A. A. Kavin, V. E. Lukash, R. R. Khayrutdinov, S. E. Bender, S. N. Kamenshikov, S. V. Konovalov, L. P. Makarova, and V. E. Zhogolev, Report ITER D_2FRCJY V1.1, 2008.
[6] C. E. Kessel, D. Campbell, Y. Gribov, G. Saibene, G. Ambrosino, R. V. Budny, T. Casper, M. Cavinato, H. Fujieda, R. Hawryluk, L. D. Horton, A. Kavin, R. Kharyrutdinov, F. Koech, J. Leuer, A. Loarte, P. J. Lomas, T. Luce, V. Lukash, M. Mattei, I. Nunes, V. Parail, A. Polevoi, A. Portone, R. Sartori, A. C. C. Sips, P. R. Thomas, A. Welander, and J. Wesley, Nucl. Fusion **49**, 085034 (2009).
[7] A. C. C. Sips, T. A. Casper, E. J. Doyle, G. Giruzzi, Y. Gribov, J. Hobirk, G. M. D. Hogeweij, L. D. Horton, A. E. Hubbard, I. Hutchinson, S. Ide, A. Isayama, F. Imbeaux, G. L. Jackson, Y. Kamada, C. Kessel, F. Koch, P. Lomas, X. Litaudon, T. C. Luce, E. Marmar, M. Mattei, I. Nunes, N. Oyama, V. Parail, A. Portone, G. Saibene, R. Sartori, J. K. Stober, T. Suzuki, S. M. Wolfe, C-Mod Team, ASDEX Upgrade Team, DIII-D Team, and JET EFDA Contributors, Nucl. Fusion **49**, 085015 (2009).
[8] G. Tardini, O. J. W. F. Kardaun, A. G. Peeters, G. V. Pereverzev, A. C. C. Sips, J. Stober, and ASDEX Upgrade Team, Nucl. Fusion **49**, 075004 (2009).
[9] V. Parail, P. Belo, P. Boerner, X. Bonnin, G. Corrigan, D. Coster, J. Ferreira, A. Foster, L. Garzotti, G. M. D. Hogeweij, W. Houlberg, F. Imbeaux, J. Johner, F. Koch, V. Kotov, L. Lauro-Taroni, X. Litaudon, J. Lonnroth, G. Pereverzev, Y. Peysson, G. Saibene, R. Sartori, M. Schneider, G. Sips, P. Strand, G. Tardini, M. Valovic, S. Wiesen, M. Wischmeier, R. Zagorski, JET EFDA Contributors, and EU ITM Task Force, Nucl. Fusion **49**, 075030 (2009).
[10] G. L. Jackson, T. A. Casper, T. C. Luce, D. A. Humphreys, J. R. Ferron, A. W. Hyatt, J. A. Leuer, T. W. Petrie, F. Turco, and W. P. West, Nucl. Fusion **49**, 115027 (2009).
[11] T. A. Casper, W. H. Meyer, G. L. Jackson, T. C. Luce, A. W. Hyatt, D. A. Humphreys, and F. Turco, "DIII-D experimental verification of model predictions for ITER startup scenarios," Nucl. Fusion (unpublished); Bull. Am. Phys. Soc. **53**, 202 (2008).
[12] P. A. Politzer, G. L. Jackson, D. A. Humphreys, T. C. Luce, A. W. Hyatt, and J. A. Leuer, Nucl. Fusion **50**, 035011 (2010).
[13] E. J. Doyle, J. C. DeBoo, J. R. Ferron, G. L. Jackson, T. C. Luce, M. Murakami, T. H. Osborne, J.-M. Park, P. A. Politzer, H. Reimerdes, R. V. Budny, T. A. Casper, C. D. Challis, R. J. Groebner, C. T. Holcomb, A. W. Hyatt, R. J. La Haye, G. R. McKee, T. W. Petrie, C. C. Petty, T. L. Rhodes, M. W. Shafer, P. B. Snyder, E. J. Strait, M. R. Wade, G. Wang, W. P. West, and L. Zeng, "Demonstration of ITER operational scenarios on DIII-D," Nucl. Fusion (to be published); *Proceedings of the 22nd IAEA Fusion Energy Conference* (IAEA, Geneva, Switzerland, 2008), Paper ex_1-3.pdf, http://www.pub.iaea.org/MTCD/Meetings/fec2008pp.asp.
[14] G. L. Jackson, T. A. Casper, T. C. Luce, D. A. Humphreys, J. R. Ferron, A. W. Hyatt, E. A. Lazarus, R. A. Moyer, T. W. Petrie, D. L. Rudakov, and W. P. West, Nucl. Fusion **48**, 125002 (2008).
[15] V. Erckmann and U. Gasparino, Plasma Phys. Controlled Fusion **36**, 1869 (1994).
[16] J. Bucalossi, P. Hertout, M. Lennholm, F. Saint-Laurent, F. Bouquey, C. Darbos, E. Traisnel, and E. Trier, Nucl. Fusion **48**, 054005 (2008).
[17] Y. S. Bae, J. H. Jeong, S. I. Park, M. Joung, J. H. Kim, S. H. Hahn, S. W. Yoon, H. L. Yang, W. C. Kim, Y. K. Oh, A. C. England, W. Namkung, M. H. Cho, G. L. Jackson, J. S. Bak, and KSTAR Team, Nucl. Fusion **49**, 022001 (2009).
[18] G. L. Jackson, M. E. Austin, J. S. deGrassie, A. W. Hyatt, J. M. Lohr, T. C. Luce, R. Prater, and W. P. West, Fusion Sci. Technol. **57**, 1 (2010).
[19] J. H. Yu and M. A. Van Zeeland, Rev. Sci. Instrum. **79**, 10F516 (2008).
[20] E. A. Lazarus, A. W. Hyatt, G. L. Jackson, and D. A. Humphreys, Nucl. Fusion **38**, 1083 (1998).
[21] B. Lloyd, G. L. Jackson, T. S. Taylor, E. A. Lazarus, T. C. Luce, and R. Prater, Nucl. Fusion **31**, 2031 (1991).
[22] C. B. Forest, Y. S. Hwang, M. Ono, G. Greene, T. Jones, W. Choe, M. Schaffer, A. Hyatt, T. Osborne, R. I. Pinsker, C. C. Petty, J. Lohr, and S. Lippmann, Phys. Plasmas **1**, 1568 (1994).
[23] V. Lukash, A. Kavin, Y. Gribov, R. Khayrutdinov, and H. Fujieda, Plasma Devices Oper. **15**, 283 (2007).
[24] L. L. LoDestro and L. D. Pearlstein, Phys. Plasmas **1**, 90 (1994).
[25] J. A. Crotinger, L. LoDestro, L. D. Pearlstein, A. Tarditi, T. A. Casper, and E. B. Hooper, "Final report to the LDRD Program," Technical Report UCRL-ID-126284, Lawrence Livermore National Laboratory, Livermore, CA (1997), available from NTIS #PB2005-102154 (1997) and http://fusion.gat.com/THEORY/caltrans/.
[26] B. Coppi and W. M. Tang, Phys. Fluids **31**, 2683 (1988).
[27] D. A. Humphreys, T. A. Casper, N. Eidietis, M. Ferrara, D. A. Gates, I. H. Hutchinson, G. L. Jackson, E. Kolemen, J. A. Leuer, J. Lister, L. L. LoDestro, W. H. Meyer, L. D. Pearlstein, A. Portone, F. Sartori, M. L. Walker, A. S. Welander, and S. M. Wolfe, Nucl. Fusion **49**, 115003 (2009).
[28] T. A. Casper, W. H. Meyer, L. D. Pearlstein, and A. Portone, Fusion Eng. Des. **83**, 552 (2008).

[29]A. A. Kavin, V. E. Lukash, R. R. Khayrutdinov, S. E. Bender, S. N. Kamenshikov, S. V. Konovalov, L. P. Makarova, and V. E. Zhogolev, Report ITER_D_233EZRQ, 2009.
[30]A. Portone, R. Albanese, G. Ambrosino, M. Ariola, A. Brooks, D. J. Campbell, T. A. Casper, M. Cavinato, V. Cuyanov, G. De Tommasi, M. Feerrara, R. Fresca, H. Fujieda, D. Gates, Y. Gribov, R. Hawryluk, I. H. Hutchinson, D. Humphreys, A. Kavin, G. D. Loesser, M. Mattei, C. Neumeyer, A. Pironti, G. Rubinacci, G. Saibee, F. Sartori, and F. Viloone, "ITER plasma vertical stabilization," *Proceedings of the 22nd IAEA Fusion Energy Conf. on Fusion Energy 2008*, Geneva, Switzerland, 2008 (IAEA, Vienna, 2008), http://www-pub.iaea.org/MTCD/Meetings/fec2008pp.asp, it_2–4ra.pdf.